PAPER

Scaling of the scrape-off layer width during inter-ELM H modes on MAST as measured by infrared thermography

To cite this article: A J Thornton *et al* 2014 *Plasma Phys. Control. Fusion* **56** 055008

IOP Publishing Plasma Physics and Controlled Fusion

Plasma Phys. Control. Fusion **56** (2014) 055008 (9pp) doi:10.1088/0741-3335/56/5/055008

Scaling of the scrape-off layer width during inter-ELM H modes on MAST as measured by infrared thermography

A J Thornton, A Kirk and the MAST Team

EURATOM/CCFE Fusion Association, Culham Science Centre, Abingdon, Oxon, 0X14 3DB, UK

E-mail: andrew.thornton@ccfe.ac.uk

Received 18 December 2013, revised 3 March 2014
Accepted for publication 27 March 2014
Published 17 April 2014

Abstract

The power load to the divertor surfaces is a key concern for future devices such as ITER, due to the thermal limits on the material surface. One factor that characterizes the heat flux to the divertor is the fall off length in the scrape-off layer (SOL), which recent empirical scalings have shown could be as small as 1 mm. These predictions are based on a multi-machine scaling of the heat flux width fitted using an expression for the divertor heat flux profile which includes a term for the exponential decay in the SOL and diffusion about the last closed flux surface (LCFS) in the private flux region. This expression has been used to fit a database of inter-ELM H mode profiles at the upper divertor and extract the fall off length, λ_q, for a range of different plasma parameters in double null plasmas. The midplane separation between the primary and secondary LCFS (δr_{sep}) of the double null plasma used in the study are in the range $2 \leqslant \delta r_{\mathrm{sep}} \leqslant 7$ mm and no correlation is seen between the fall off length and the δr_{sep}. The MAST data shows good agreement with the formula, with the fitted fall off length spanning a range of 5–11 mm in the data base generated. Regression of this data has shown that the fall off length has the strongest dependence on the plasma current (or equivalently, the poloidal magnetic field at the outboard midplane) to the power −0.71. The scaling with the smallest χ^2 error utilizes the poloidal magnetic field at the outboard midplane ($B_{\mathrm{pol,omp}}$) and the power crossing the SOL in the relation $\lambda_q(\mathrm{mm}) = 1.84(\pm 0.48)\mathrm{B}_{\mathrm{pol,omp}}^{-0.68(\pm 0.14)}\mathrm{P}_{\mathrm{SOL}}^{0.18(\pm 0.07)}$ with $\chi^2 = 3.46$ and $R^2 = 0.56$ as a goodness of fit. The equivalent scaling with plasma current is $\lambda_q(\mathrm{mm}) = 4.57(\pm 0.54)\mathrm{I}_{\mathrm{p}}^{-0.64(\pm 0.15)}\mathrm{P}_{\mathrm{SOL}}^{0.22(\pm 0.08)}$ with $\chi^2 = 3.84$ and $R^2 = 0.55$. The moderate goodness of fit suggests that additional plasma parameters are required to accurately reproduce the observed variation in λ_q.

Keywords: heat flux widths, scrape-off layer, scaling, MAST, spherical tokamak, infrared

(Some figures may appear in colour only in the online journal)

1. Introduction

The power leaving a tokamak plasma is directed along the scrape-off layer (SOL) and onto the divertor surfaces by the magnetic field geometry. The width of the SOL region is of key importance to future devices such as ITER as it sets the size of the parallel heat flux. In ITER it is expected that the power crossing the SOL will be of the order 100 MW [1]. Initial predictions for ITER based on modelling results have suggested that the inter-ELM H mode fall off length in the SOL, λ_q, will be of the order 5 mm [2]. Recent work [3] has shown that this size could be as small as 1 mm. Taking into account the magnetic geometry of ITER, a heat flux width of 5 mm will give a parallel heat flux of 1 GW m^{-2}, which is higher than on present day devices. The divertor is designed to minimize the surface heat flux to the plasma facing components, via tile inclination and radiation of the power passing along the divertor leg, to levels of the order 10 MW m^{-2} in steady state. In the case where the fall off length is 1 mm, then the heat flux rises significantly and could lead to damage to the divertor materials, limiting the lifetime of the ITER divertor.

The measurement of the fall off length is typically made using infrared (IR) thermography or Langmuir probe (LP) measurements. The measured heat flux is fitted using a range of different techniques to extract the fall off length. Recent work [3–5] has developed a model of the heat flux which corresponds to an exponential decay in the SOL region and the diffusion of power across the last closed flux surface (LCFS) and into the private flux region (PFR) along the divertor leg [6]. It is this work, using the new model of the heat flux profile, which has suggested that λ_q in ITER is of the order 1 mm. In these studies and those that have used only an exponential decay in the SOL region for the fitting [7], the factor with the strongest effect on λ_q is the magnitude of the poloidal magnetic field, B_p. It is typically found that λ_q scales as B_p^{α} where α ranges from -1.5 to -0.9.

This paper will use IR data from MAST [8] to generate a scaling for the inter-ELM H mode fall off length in double null plasmas as a function of various plasma parameters. The fall off length will be determined using the method set out by Eich *et al* [3] in which the measured heat flux profile, q, measured at the upper divertor is fitted with equation (1). The work presented here follows on from work previously performed on MAST using LP data and general agreement is found between the two data sets.

$$q(\bar{s}) = \frac{q_0}{2}\exp\left(\left(\frac{S}{2\lambda_q \cdot f_x}\right)^2 - \frac{\bar{s}}{\lambda_q \cdot f_x}\right) \times \mathrm{erfc}\left(\frac{S}{2\lambda_q \cdot f_x} - \frac{\bar{s}}{S}\right) + q_\mathrm{bg}. \quad (1)$$

In equation (1), $\bar{s} = (R - R_0)$ with R_0 the location of the LCFS, f_x is the flux expansion from the outboard midplane to the divertor surface, q_0 is the heat flux at the outboard midplane, S is the power spreading parameter and is the width of the Gaussian and q_bg is the background heat flux. All of these parameters are fitted, with the exception of the flux expansion to obtain a value for the heat flux fall off length at the midplane, λ_q. The flux expansion is determined using the variation of the magnetic field at the divertor and the outboard midplane, as determined by EFIT equilibrium reconstruction [9].

The structure of the paper will be as follows; section 2 will outline the method used to measure the heat flux profiles and the stages used to generate a database of plasma parameters which will be used to determine the scaling. Section 3 will discuss the scaling of the fall off length with individual upstream plasma parameters and identify the parameters which have the largest effect on setting λ_q and act as a guide as to the regressions performed. Section 4 will focus on regressing the variables chosen in section 3 to give a relationship for the fall off length. Finally, the paper will conclude with a discussion in section 5.

2. SOL width database

The database generated for this study focuses on inter-ELM measurements of the upper outer divertor heat flux of attached double null plasmas. The choice of discharge and divertor surface on which to measure the heat flux has been dictated by the availability of IR data during the MAST campaign. The measurements of the heat flux have been taken during a period

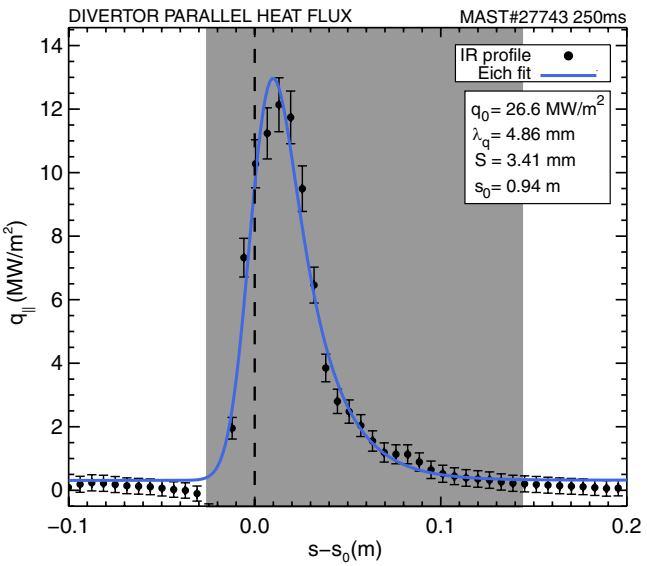

Figure 1. The measured heat flux profile at the upper outboard divertor (black dots) with the fit using the Eich formula (blue curve). The shaded region signifies the region over which the IR profile is fitted to determine the fall off length; a range $3 \cdot S$ wide on the private flux region and $7(S + \lambda_q)$ on the SOL side. The fitted fall off length (λ_q), parallel heat flux at the midplane, q_0, and Gaussian spreading factor, S, are shown for this profile.

where only one of the IR cameras was operational, and the use of double null, upper divertor data provides the largest dataset for analysis. In double null plasmas it is possible to generate both ELMing and ELM free discharges, both types of which are included in the database. It should be noted that the strike point footprint broadens during ELMs [10] which will affect the calculated value of λ_q. In order to avoid the effects of ELM broadening, the profiles have been selected which are at least 1.2 ms after an ELM, as measured using divertor D_α emission. The duration of 1.2 ms is taken as this is twice the ELM heat flux decay time, as measured in ELMy double null MAST plasmas [11] and ensures that the plasma has recovered from the ELM. It should be noted, that whilst the ELMs have been excluded from the analysis, they do still deposit a broad heat flux to the target which will affect the time-varying surface temperature.

The heat flux to the divertor in MAST is routinely measured using IR thermography [7]. A typical IR profile for the divertor heat flux is shown in figure 1 with the measured heat flux converted into the parallel heat flux. The profiles at the selected period are fitted using equation (1), first over the whole profile to enable a suitable range for the fitting to be defined. The initial fit is used to determine the width of the Gaussian and an estimate for the fall off length. The profile is then refitted using a range which is three Gaussian widths wide in the PFR and $7(S + \lambda_q)$ on the SOL side of the profile. These ranges were chosen as it would be expected that three Gaussian widths would encompass 99% of the profile on the PFR side and the SOL side width was chosen as it provides an acceptable level for the background heat flux (q_bg).

The fits are filtered based on the chi-square (χ^2) of the fit and then manually inspected to ensure the profiles are accurately fitted. The fitted parameters, along with plasma

Table 1. Range of plasma parameters included in the database.

Parameter	Range	Units
B_{pol}	0.11–0.23	Tesla
B_{tor}^{vac}	0.36–0.41	Tesla
I_p	0.45–0.92	MA
n_{line}	1.16–2.58	$\times 10^{20}$ m^{-2}
P_{SOL}	0.84–4.42	MW
P_{NBI}	0–3.8	MW
P_{rad}	0.1–0.7	MW
f_{GW}	0.37–0.85	—
R_{geo}	0.897–0.991	m
q_{95}	4.7–9.1	—

parameters such as the line integrated density (n_{line}), power crossing the SOL determined from power balance (P_{SOL}), plasma current (I_p), vacuum toroidal magnetic field at the geometric axis (B_{tor}^{vac}) and the poloidal field at the outboard midplane (B_{pol}^{omp}), major radius of the magnetic axis (R_{geo}), Greenwald fraction (f_{GW}), safety factor at 95% of the poloidal flux (q_{95}) are stored for each IR profile fitted. Table 1 shows the ranges in the plasma parameters for the 139 profiles that form the database.

The fall off length from equation (1) is one of several methods of quantifying the heat flux width. An alternative method is the integral width, λ_{int}, and is defined in equation (2) [12]. It has been shown [4] that the integral width and the fall off length are related by the formula $\lambda_{int} = \lambda_q + 1.64 \cdot S$ when the Eich fit is a good representation of the heat flux profile [5] and that $S/(2 \cdot \lambda_q) < 1$ is satisfied [4]. The relation between λ_{int} and λ_q provides an additional means of verifying the accuracy of the fit. The integral width is plotted against $\lambda_{int} = \lambda_q + 1.64 \cdot S$ in figure 2 for the profiles used in the database.

$$\lambda_{int} = \int_{\text{fit range}} \frac{q(s) - q_{bg}}{\max(q(s) - q_{bg})} \mathrm{d}s \,. \qquad (2)$$

Figure 2 clearly shows a strong correlation between the fall off length from the Eich formula and the integral width, thereby confirming the quality of the fits used in the database, though it is clear that there is some scatter in the points of order 10–15%, which could affect the later regression. The requirement for $S/(2 \cdot \lambda_q) < 1$ should also be checked to ensure that the relationship between λ_q and λ_{int} is applicable to the dataset, which is confirmed by figure 3. The scatter present in figure 2 is also present in figure 3, which is to be expected as the values in the figure are extracted from the Eich fit.

2.1. Surface effects on the measured IR profiles

The measurement of the heat flux to the divertor using IR thermography is affected by the presence of surface layers or surface irregularities. The effects of surface layers on IR measurements have been well documented [7, 13, 14] and are seen to generate negative heat fluxes following short energy pulses (e.g. after ELMs) as a result of the rapid heating experienced by a thin layer in good thermal contact with the bulk divertor material. It is important to understand the effects of surface layers on the measured fall off lengths, as this could impact the reliability of the scaling that has been determined.

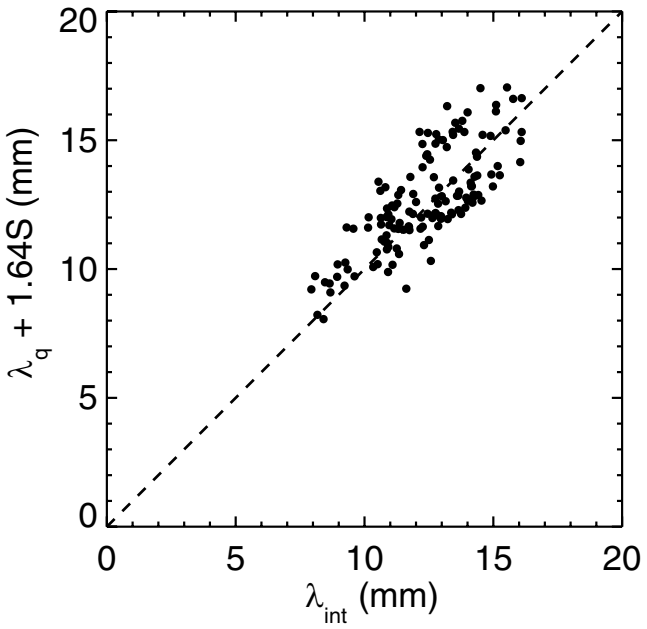

Figure 2. Comparison of the integral heat flux width and the $\lambda_q + 1.64S$ scaling derived from the Eich fit.

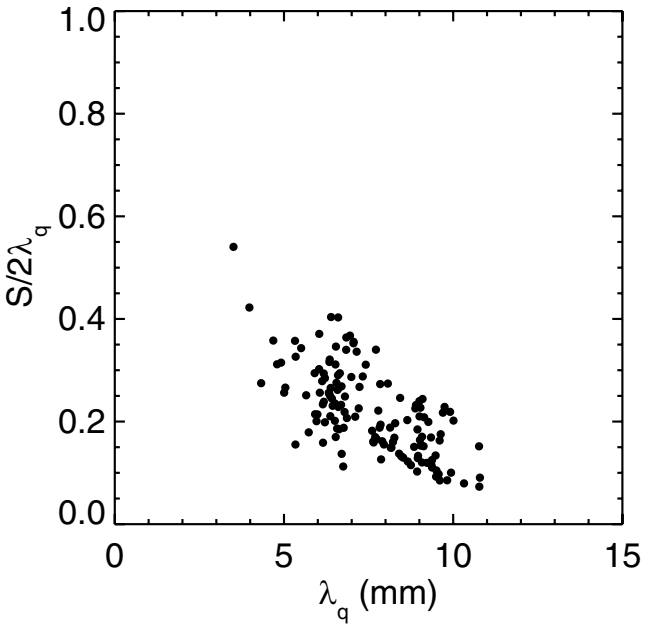

Figure 3. Variation of the Gaussian spreading factor, S, with the fitted fall off length λ_q.

The surface layer coefficient for the divertors on MAST has been determined previously [7] using cross checking between two different wavelength cameras and using energy balance arguments. The optimum value of the surface layer coefficient, α was determined to be 70 kW m^{-2} K^{-1} and this value has been used in this analysis. It should be noted that the α value used is taken to be constant across the surface of the divertor target, which may not necessarily be the case due to the effect of erosion and deposition. The use of α in these studies, as in other such studies, is as an average parameter to calibrate the diagnostic results and is not a physical heat diffusion coefficient of the surface layer on the divertor.

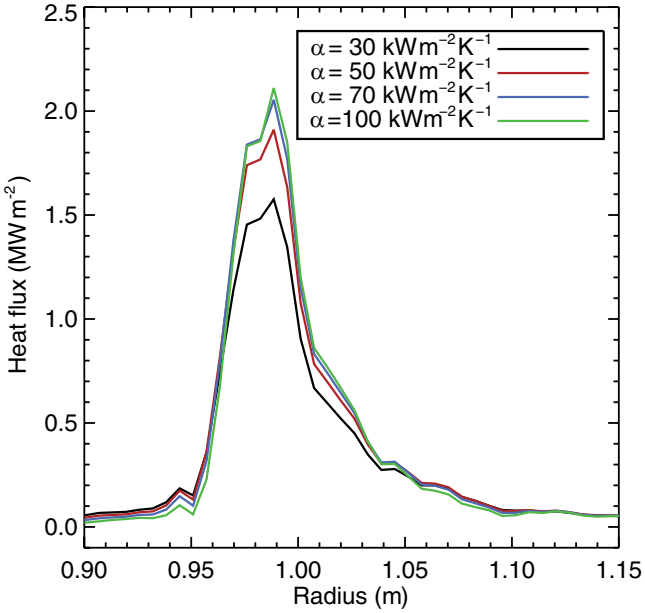

Figure 4. Measured inter-ELM heat flux profiles calculated using a range of surface layer coefficients, α.

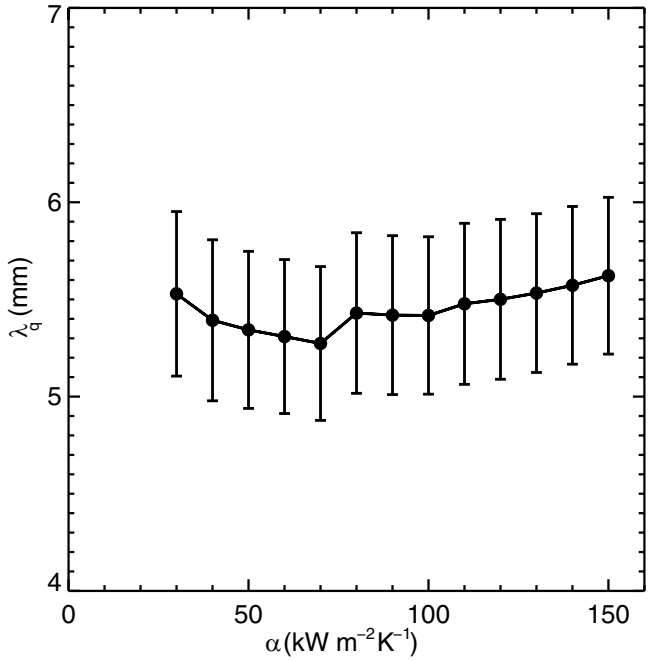

Figure 5. The variation of the fitted fall off length, λ_q, as a function of the surface layer coefficient α.

In order to gain a greater understanding on the effect of the surface layer coefficient of the fall off length, an ELM free discharge was taken and a range of α used from 30 to 200 kW m^{-2} K^{-1} to calculate the heat flux to the divertor. Figure 4 shows the heat flux profiles at a given time in the discharge as a function of α. It is clear that the surface layer correction has a significant effect on the calculated peak heat flux to the divertor. The profiles in figure 4 are then fitted to determine the fall off length for each of the α values used, which is plotted in figure 5. It is clear from figure 5 that whilst the peak of the heat flux is affected by the chosen α, the fall off length is unaffected with the fitted fall off length for all α lying within the error returned from the fit.

3. Scaling of the SOL width

In this section, the correlation between the variables in the database will be investigated and variation with one parameter, holding the others fixed, will be found which will act to guide which parameters can be used in the final regression.

The strongest scaling of the fall off length found in many studies is with the plasma current, I_p [5, 15]. The variation of the fall off length with the plasma current is shown in figure 6. As the data shown in figure 6 shows all of the data points in the database, there is a range of different plasma densities and power crossing the SOL which gives rise to scatter in the points at a given plasma current. The variation in the density and the power crossing the SOL for the data set is shown in figures 8 and 7. The density of the plasma, as determined from interferometer measurements has been seen to affect the fall off length in other studies on MAST [16, 17] where LP data was used to determine the heat flux to the divertor. These studies have also shown the power crossing the SOL can have an effect on the measured fall off length.

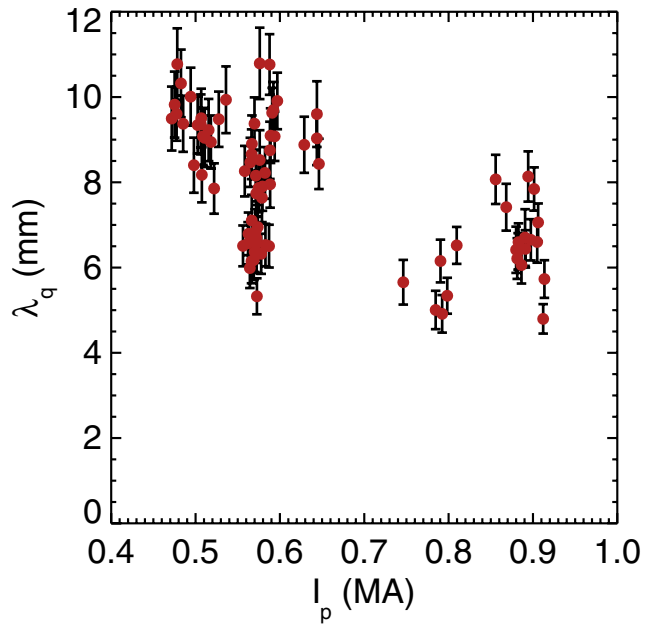

Figure 6. The variation of the fitted fall off length, λ_q, as a function of the plasma current, I_p.

The dependence of the fall off length on the plasma current can be investigated by selecting data points at constant P_{SOL} and density and determining the dependency of λ_q on plasma current for these points.

Figure 9 shows the scaling of the fall off length at fixed P_{SOL} (black circles), and for three different selections of fixed density (green plus sign, gold triangle and purple crosses). The constant P_{SOL} values correspond to the blue squares on figure 7 and the fixed density data correspond to the points in figure 8. The data points here show a clear trend of decreasing λ_q for increasing plasma current. Due to the limitations of the data set, it is not possible to choose data points of fixed

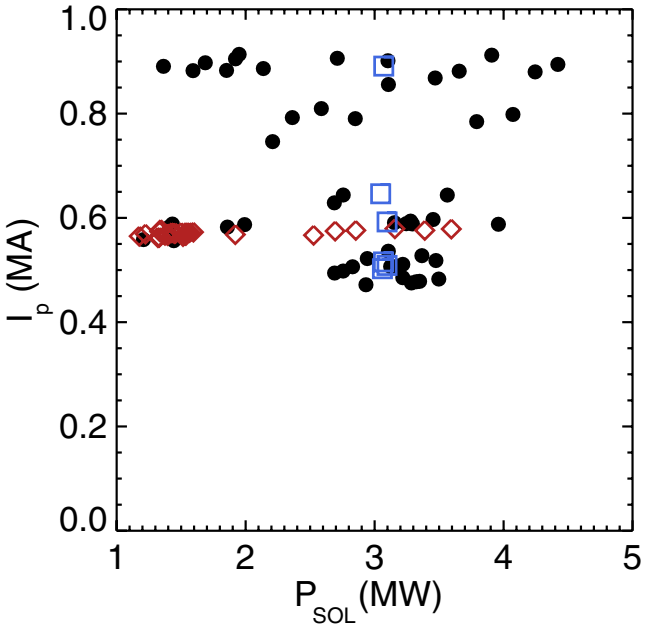

Figure 7. Correlation of the power crossing the SOL (P_{SOL}) and the plasma current. The red diamonds correspond to a subset of the data where the P_{SOL} is allowed to vary and the blue squares correspond to a subset of the data where the plasma current is allowed to vary at fixed P_{SOL}.

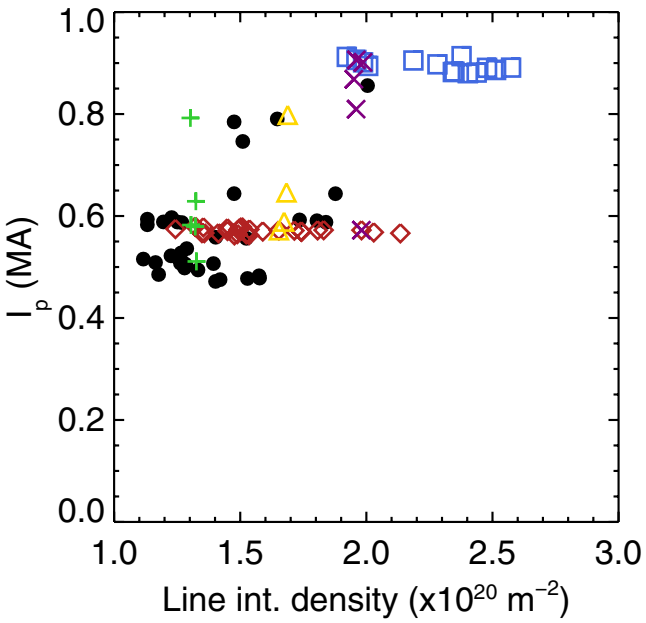

Figure 8. Correlation of the line integrated density in the plasma, as measured by interferometer, and the plasma current (I_{p}). The red diamonds are a subset of this data where the plasma current is constant ($I_{\mathrm{p}} \approx 600$ kA) and the blue squares are a subset at a higher plasma current of 900 kA. The points shown by the green plus, purple cross and gold triangle are points at fixed density and varying plasma current.

density and P_{SOL} and as a result scatter from this variation is present in the data in figure 9. The points at the three different densities support the variation seen at fixed P_{SOL}, but they do not show a clear dependence of λ_q on the density. The reduced χ^2 of the power law fit is 0.92. A linear fit can also be made to the data shown in figure 9, which gives a fit of

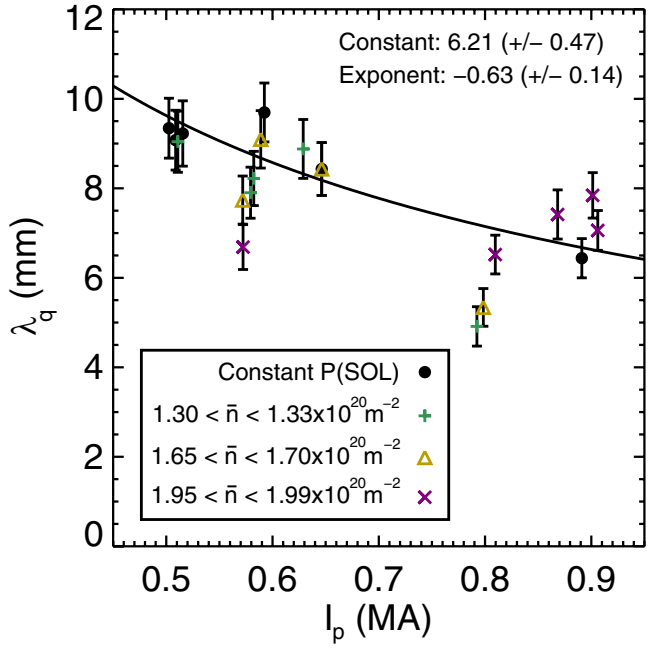

Figure 9. Scaling of the fall off length with the plasma current at a fixed value of P_{SOL} (black circles) and fixed densities (green plus, purple crosses and gold triangles). The fit to the data is of the form $y = A * I_{\mathrm{p}}^{b}$, where A is the constant and b is the exponent shown on the figure.

$\lambda_q = 13.4(\pm 1.0) - 7.62(\pm 1.51) I_{\mathrm{p}}$ with reduced $\chi^2 = 0.57$ which suggests the data is better represented as a power law.

The variation of the fall off length with the density can be investigated further by selecting a range of data points at constant plasma current. The chosen points are shown in figure 8 for a plasma current of 600 kA (red diamonds) and 900 kA (blue squares) respectively. It is clear to see that there is a positive relationship between the plasma current and density which is due to the existence of the Greenwald density limit [18], whereby higher density plasmas stable at higher current. Figure 10 shows the variation of the fall off length with the density for each of these two plasma currents. The dependence of λ_q is shown if the average of the 600 kA and 900 kA points are taken, whereby the 600 kA points have a larger λ_q than the points at 900 kA. The scaling of the fall off length with the density is not clear from figure 10, there is a weak dependence based on the smaller variation seen in λ_q for the higher density points compared to the lower density points. There is a range of P_{SOL} values for the data shown in figure 10 which could affect the variation seen.

The power crossing the SOL is a variable which has been seen to affect the fall off length in several recent studies [5, 17]. In figure 7 the power crossing the SOL, P_{SOL}, is plotted as a function of the plasma current to determine if there is a correlation between these two parameters. The P_{SOL} value is largely uncorrelated with the plasma current, which permits all of the data collected to be used in the scaling as there is a range of input power for a given plasma current.

To identify if there is a scaling of the fall off length with P_{SOL}, a region of data is selected at constant plasma current as λ_q is known to vary with this quantity. The scaling of the

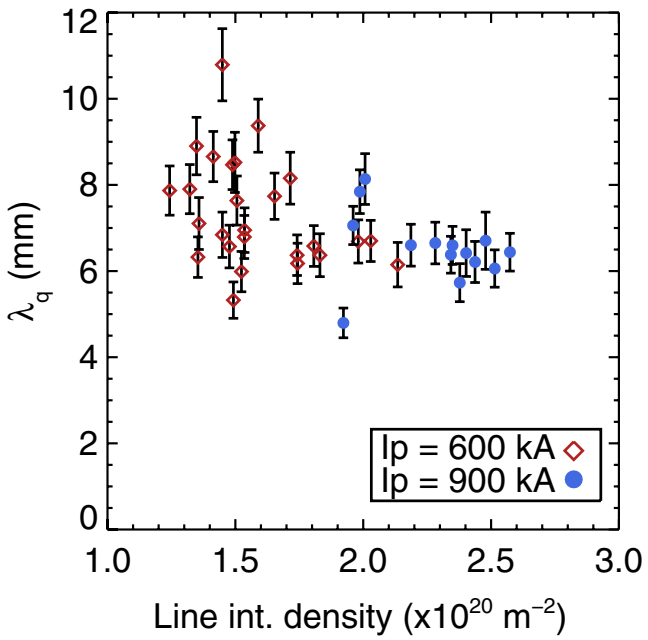

Figure 10. The variation of the fall off lengths, λ_q, as a function of the line integrated density for two different plasma currents. Data with a plasma current at 600 kA is shown by the red diamonds and data from plasmas with a current of 900 kA is shown by the blue circles.

fall off length with P_{SOL} can be found using this subset of data (red diamonds in figure 7) and the power crossing the SOL is allowed to vary. The variation of λ_q with P_{SOL} in this subset of the data is weak. There are a significant number of points at $\lambda_q = 6.5$ mm and $P_{\mathrm{SOL}} = 1.4$ MW which dominate the fit, reducing these to one single point effectively eliminates the dependence of λ_q on P_{SOL}. Previous studies on MAST [17] and recent multi-machine scalings [5] show a weak positive scaling with P_{SOL}.

For the toroidal magnetic field, B_{t}, one can use either the magnetic field returned from equilibrium reconstruction at the magnetic axis of the plasma, or the vacuum magnetic field at the geometric centre of the tokamak. In the case of the magnetic field returned from equilibrium reconstruction, there is a strong correlation between the toroidal field and the poloidal field at the outboard midplane. The strong correlation and wide variation in the toroidal field at the axis is due to the effect of β_{p} on the plasma. The β_{p} affects whether the plasma is diamagnetic ($\beta_{\mathrm{p}} < 1$) or paramagnetic ($\beta_{\mathrm{p}} > 1$) which in turn changes the toroidal field on axis. In order to remove the interdependence, and remain in line with other SOL width scalings [17] and confinement scalings [19], the vacuum field at the geometric axis is used as the toroidal magnetic field. The database contains a limited variation in the vacuum B_{t}. There is some variation in the fall off length with the vacuum B_{t}, however, the data is inconclusive and based on a small sample of the data. Essentially all of the points in the scaling are at the same value of B_{t}, taking this into consideration, along with the results of other studies where the toroidal field is seen to have only a weak scaling with the fall off length [4, 5, 17], the vacuum B_{t} will not form part of the regression.

4. Regression of SOL width to input parameters

The regression of the fall off length with the plasma parameters is performed to a power law fit of the form $\lambda_q = C \cdot A^a B^b$ where C is a constant, A–B are the plasma parameters and the powers of the fit are given by a–b. The regression of the parameters is performed in linear space by least squares fitting. Regression in linear space allows better handling of the error on the fitted λ_q than performing the regression in log space and has been applied in previous scalings on MAST [17] and multi-machine datasets [5]. The results from the individual parameter scalings determined in section 3 are used to guide the parameters used in the regression. The fall off length is seen to exhibit a strong scaling with the plasma current, therefore the plasma current is used as a regression variable. Correspondingly, as the plasma current and the poloidal field are related, the plasma current can be replaced in the regression with the poloidal magnetic field at the outboard midplane (B_{pol}). The result of the regressions are shown in table 2, with regressions 1 and 2 showing the difference between regressing against I_{p} and $B_{\mathrm{pol,omp}}$ respectively. A regression against the line integrated density is also included, as a weak dependence of the fall off length on density was seen for the studies of the individual parameters. The error in the regression exponents is returned from the least squares fitting routine used to regress the quantities. The standard error derived from a χ^2/dof (reduced chi squared) value, where dof is the number of degrees of freedom, assumes that the fit gives $\chi^2/dof = 1$. When the χ^2/dof is large, as is the case for the fitted quantities here, only a small variation in the parameters will cause the reduced chi squared to change by 1, leading to underestimates on the errors in the fitted quantities. In the case of a large reduced chi squared for the fit, the error in the regressed variables can be better estimated for by multiplying the error value returned by the reduced chi square of the fit, it is this value that is quoted as the error in the exponent.

The regression of the data shows that the strongest dependence is on the poloidal magnetic field at the outboard midplane, however, the difference between the exponent on this regression variable and the plasma current is within the error range on the exponent. The value for the plasma current dependence is within 15% of the studies previously performed in H mode in MAST when all the data points are included [17], but it should be noted that the plasma current range in the data set here is larger than that previously used. There is some variation of the magnitude of the scaling when compared with other machines, especially NSTX [4, 15] which shows a stronger dependence (-1.33 to -1.6 in exponent), though this is over a larger range of plasma current than in the dataset presented in this paper. The P_{SOL} scaling is consistent with previous MAST studies, and those seen across a range of devices [5]. The exponents in the regression match well with the exponents of the fits to the selected data in section 3, which confirms that the regression is consistent with the fits when one parameter is varied in isolation. The quality of the fit is moderate for the regressions presented here, the best fit is obtained using the poloidal field and this gives the fall off length to be as shown in equation (3).

$$\lambda_q(mm) = 1.84(\pm 0.48) B_{\mathrm{pol,omp}}^{-0.68(\pm 0.14)} P_{\mathrm{SOL}}^{0.18(\pm 0.07)}. \quad (3)$$

Table 2. Parameters for each of the regression variables.

Reg.	Const.	B_{pol}^{omp} (T)	I_p (MA)	P_{SOL} (MW)	n_{line} $\times 10^{20}$ m^{-2}	R^2	χ^2
1	4.57 (±0.54)	—	−0.64 (±0.15)	0.22 (±0.08)	—	0.55	3.84
2	1.84 (±0.48)	−0.68 (±0.14)	—	0.18 (±0.07)	—	0.56	3.46
3	4.03 (±0.88)	—	−0.75 (±0.23)	0.24 (±0.08)	0.14 (±0.19)	0.56	3.81

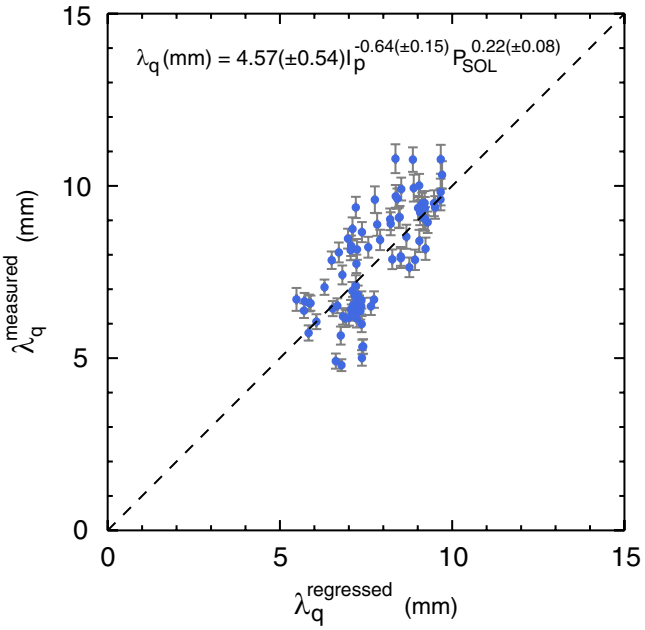

Figure 11. Regression of the measured lambda with most significant plasma parameters (I_p and P_{SOL}).

Whilst the regression in equation (3) is the fit with the smallest χ^2 error, the typical scaling parameter for the fall off length is the plasma current. The plasma current is widely used across a range of different machines, and is independent of the location chosen to be the outboard midplane. Therefore, the regression including the plasma current (regression 1, equation (4)) should be quoted to allow convenient comparison between the MAST studies presented here and the scalings from elsewhere.

$$\lambda_q(mm) = 4.57(\pm 0.54) I_p^{-0.64(\pm 0.15)} P_{SOL}^{0.22(\pm 0.08)}. \quad (4)$$

The measured fall off length, $\lambda_q^{measured}$ can be plotted against the regressed fall off length, $\lambda_q^{regressed}$, which is shown in figure 11 to confirm the fitted data accurately represents the measured values.

The regression has also been performed including the density (regression 3). The regression shows a weak dependence with density, with the exponent of the density having the largest relative error of all of the regressed parameters. The fit quality is not improved by the inclusion of the density, remaining similar to the regression including only I_p and P_{SOL}. The addition of the density into the regression increases the strength of the scaling with plasma current. This increase is likely due to the operational constraints in MAST by which higher density plasma are performed at higher currents which is consistent with the Greenwald scaling [18]. The density dependence from the regression also differs in sign from that expected from the analysis in section 3, but is consistent in sign when compared to other studies on MAST [17]. The magnitude of the density dependence found in these studies is much weaker than seen in past MAST data. These previous studies of the fall off length on MAST [16, 17] have used LPs to derive the heat flux to the divertor. The derivation of the heat flux from LP data requires an assumption to be made about the ion temperature (T_i) to determine the sheath heat transmission coefficient. It was assumed in previous studies of the SOL width derived from LP data that the ion (T_i) and electron temperatures (T_e) were equal, and this is then used to derive the heat flux to the divertor. Measurements of T_i at the divertor have shown that this is not the case [20], especially in the case of low collisionality discharges where there is little coupling between the ions and electrons through collisions. The poor coupling at low density leads to ion temperatures higher than electron temperatures. Therefore, assuming that the ion and electron temperatures are the same would cause the profile to be narrower than was actually the case, thereby making the density dependence stronger. Taking into consideration the observation that T_i/T_e decreases with increasing collisionality [20], then this would act to broaden the profiles at lower density and lessen the density dependence, thus making the LP data more consistent with the SOL width scaling derived from the IR data.

4.1. Power spreading factor

The power spreading factor, S, in the Eich fit becomes the dominant contribution to the integral fall off length as λ_q decreases in size. The contribution from the power spreading factor to the integral width was highlighted in section 2, where the relation $\lambda_{int} = \lambda_q + 1.64 \cdot S$ [4] was discussed. For example, in ITER, where predictions suggest that $\lambda_q = 1$ mm [3], the integral width would be dominated by S if the spreading parameter is of order the fall off length, which was previously noted in [5].

The variation of the power spreading factor with the fall off length for the data used in this paper is shown in figure 12. There is little variation of the spreading parameter with the fall off length and the data points are located in a range between 2 and 5 mm, which is consistent with NSTX data and previous MAST studies [5], but is larger than measurements from conventional aspect ratio devices by between a factor 2 to 3. The fact that the fitted S parameter comes from a dataset with a range of plasma parameters and yet shows a similar values for all fall off lengths suggests that other parameters, such as the design and mode of operation of the divertor determine the level of diffusion occurring between the X point and the target.

Analysis of data from other machines [5, 21] has shown that the power spreading factor is similarly grouped around a

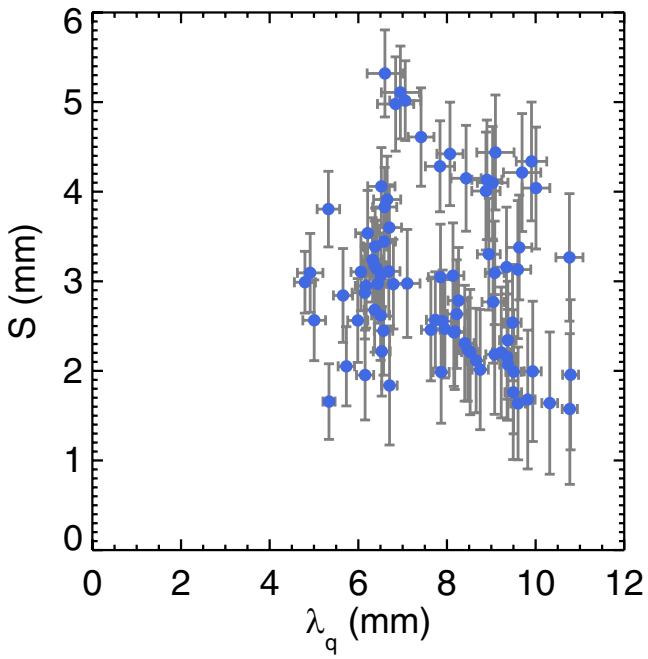

Figure 12. The variation of the power spreading factor, S, with the SOL fall off length, λ_q, for the data used in the regression.

specific value for a given machine, and the power spreading factor is not affected by the choice of wall material between carbon and tungsten [21]. A significant change in S can be seen when the divertor geometry is changed, as can be seen between DIV-I and DIV-II data from ASDEX-Upgrade [21]. These results suggest that increased divertor closure generates larger power spreading parameters, an observation which could be key in predicting the S value for MAST-Upgrade. In addition, theoretical work [22] has suggested that increasing the connection length would lead to increased diffusion and the power spreading parameter dominating the fall off length. If it is the case that divertor closure and increased connection lengths give rise to enhanced S values, then this would suggest that the dominant part of the heat flux profile in MAST-Upgrade would come from diffusion and S would exceed λ_q.

The power spreading factor in MAST is not seen to scale with any statistical significance with the pedestal density or poloidal magnetic field, unlike as reported in other studies [21]. Correlation of the S parameter and either of these two parameters for the MAST data suggests that they are only able to account for approximately 10% of the variation seen in the S value. It is clear from these considerations, as has already been suggested [5], that a multi-machine investigation of the scaling of S is required, without such work and subsequent scaling, extrapolation of the power spreading factor MAST-Upgrade or ITER will not be possible.

5. Discussion

The divertor heat flux has been measured on MAST using IR thermography in a range of inter-ELM H mode discharges. The IR measurements of the heat flux profile have then been fitted using the Eich formula, which includes a Gaussian diffusion term to account for diffusion of the heat about the LCFS and an exponential fall off to account for the SOL decay. The Eich formula allows the fall off length at the midplane, λ_q to be extracted by accounting for the flux expansion from the midplane to the target. The Eich fall off length has been seen to be related to the integral width, which is widely used elsewhere, by Makowski *et al* [4] and the MAST results support this relation which was derived from other conventional tokamaks and NSTX. The confirmation of this result has been used as a means of testing for a good fit to the heat flux profile, and allowing the selection of a reliable dataset for further analysis. An investigation has been performed into the effect of the surface layer coefficient (α) on the observed heat flux width, which can have a significant effect on the heat flux profiles returned from IR measurements [7]. The fall off length has been fitted for the same heat flux profiles, using a range of different surface layer coefficients and this has shown that the variation in the fall off length as a result of changing the α is within the error on the fitted fall off length. Hence, the α value is not a significant factor in the determination of the fall off length.

The fall off length has been measured for a range of different plasma parameters such as poloidal magnetic field, toroidal field, density and power crossing the SOL (P_{SOL}). The scaling of the fall off length against individual plasma parameters has been used to determine if a given parameter affects the fall off length at all, and to determine the quantities most suitable for regression. The strongest dependence is seen on the plasma current (or equivalently the poloidal magnetic field at the outboard midplane). The fall off length is seen to narrow with increasing plasma current, which is consistent with data from other devices. There is a weak scaling of the fall off length on the power crossing the SOL, in which higher values of P_{SOL} give rise to larger fall off lengths. The dataset does not include sufficient data points at varying toroidal magnetic field to enable an accurate scaling with this quantity to be determined. These dependencies seen in the individual scalings of the fall off length are borne out when a multiple parameter regression is performed across the dataset. The low confidence level of the good fit suggests an additional parameter is required to fully explain the variation of the fall off length. The use of the scaling found to predict a fall off length for MAST-Upgrade would give $\lambda_q^{\mathrm{MAST\text{-}U}} = 5.1$ mm, at the maximum plasma current of 2 MA and full heating power of 12.5 MW planned at then end of the upgrade. It is possible that this additional parameter could be the pedestal electron temperature, however, further work will be required to obtain high resolution Thomson scattering data around the LCFS location to accurately test this hypothesis. Obtaining such measurements of the electron temperature will enable the heat flux fall off width from the IR to be compared to the midplane fall off length in the electron temperature. These quantities should be related from simple SOL physics understanding and from the operating regime, either sheath limited or conduction limited SOL, for a given plasma [23]. In addition, it has been seen that inter-ELM filaments arrive at the divertor [24] and it could be that the arrival of the filaments at the divertor plays a role in determining the λ_q. Investigation of the arrival of the filaments would require high speed visible imaging of

the divertor to determine if a filament has arrived during the integration time of the IR camera and will be the subject of future work.

A key issue for the extrapolation of the integral width to future devices such as MAST-Upgrade or ITER is prediction of the power spreading factor, S.

Acknowledgments

This work was part funded by the RCUK Energy Programme [grant number EP/I501045] and the European Communities under the Contract of Association between EURATOM and CCFE. To obtain further information on the data and models underlying this paper please contact PublicationsManager@ccfe.ac.uk. The views and opinions expressed herein do not necessarily reflect those of the European Commission. The authors would also like to thank Dr G Arnoux and Professor B Lipschultz for their helpful comments and suggestions.

References

[1] Loarte A *et al* 2007 Progress in the ITER Physics Basis. Chapter 4: Power and particle control *Nucl. Fusion* **47** S203–63
[2] Kukushkin A S *et al* 2003 Scaling laws for edge plasma parameters in ITER from two-dimensional edge modelling *Nucl. Fusion* **43** 716
[3] Eich T *et al* 2011 Inter-ELM power decay length for JET and ASDEX Upgrade: measurement and comparison with heuristic drift-based model *Phys. Rev. Lett.* **107** 215001
[4] Makowski M A *et al* 2012 Analysis of a multi-machine database on divertor heat fluxes *Phys. Plasmas* **19** 056122
[5] Eich T *et al* 2013 Scaling of the tokamak near the scrape-off layer in H-mode power width and implications for ITER *Nucl. Fusion* **53** 093031
[6] Wagner F 1985 A study of the perpendicular particle transport properties in the scrape off layer of ASDEX *Nucl. Fusion* **25** 525–36
[7] De Temmermann G *et al* 2010 Thermographic studies of heat load asymmetries during MAST L-mode discharges *Plasma Phys. Control. Fusion* **52** 095005
[8] Meyer H *et al* 2013 Overview of physics results from MAST towards ITER/DEMO and MAST Upgrade *Nucl. Fusion* **53** 104008
[9] Lao L L *et al* 1985 Reconstruction of current profile parameters and plasma shapes in tokamaks *Plasma Phys. Control. Fusion* **25** 1611
[10] Eich T *et al* 2011 Type-I ELM power deposition profile width and temporal shape in JET *J. Nucl. Mater.* **415** S856–9
[11] Thornton A J *et al* 2014 The effect of resonant magnetic perturbations on the divertor heat and particle fluxes in MAST *Nucl. Fusion* in press
[12] Loarte A *et al* 1999 Multi-machine scaling of the divertor peak heat flux and width for L-mode and H-mode discharges *J. Nucl. Mater.* **266–269** 587–92
[13] Herrmann A *et al* 2001 Limitations for divertor heat flux calculations of fast events in tokamaks *27th Conf. on Plasma Physics and Controlled Fusion (Madeira, Portugal) Proc. EPS 2001*
[14] Delchambre E *et al* 2009 Effect of micrometric hot spots on surface temperature measurement and flux calculation in the middle and long infrared *Plasma Phys. Control. Fusion* **51** 055012
[15] Gray T K *et al* 2011 Dependence of divertor heat flux width on heating power, flux expansion and plasma current in NSTX *J. Nucl. Mater.* **415** S360–4
[16] Ahn J-W *et al* 2006 L-mode SOL width scaling in the MAST spherical tokamak *Plasma Phys. Control. Fusion* **48** 1077–92
[17] Harrison J R *et al* 2013 L-mode and inter-ELM divertor particle and heat flux width scaling on MAST *J. Nucl. Mater.* **438** S375–8
[18] Greenwald M *et al* 2002 Density limits in toroidal plasmas *Plasma Phys. Control. Fusion* **44** R27–80
[19] McDonald D C *et al* 2007 Recent progress on the development and analysis of the ITPA global H-mode confinement database *Nucl. Fusion* **47** 147
[20] Elmore S *et al* 2013 Scrape-off layer ion temperature measurements at the divertor target in mast by retarding field energy analyser *J. Nucl. Mater.* **438** S1212–5
[21] Sieglin B *et al* 2013 Power load studies in JET and ASDEX-Ugrade with full-W divertors *Plasma Phys. Control. Fusion* **55** 124039
[22] Goldston R 2010 Downstream heat flux profile versus midplane T profile in tokamaks *Phys. Plasmas* **17** 012503
[23] Stangeby P C 2000 *The Plasma Boundary of Magnetic Fusion Devices* (London: Taylor and Francis)
[24] Ben Ayed N *et al* 2009 Inter-ELM filaments and turbulent transport in the Mega-Amp Spherical Tokamak *Plasma Phys. Control. Fusion* **51** 035016